OPEN ACCESS
IOP Publishing
Superconductor Science and Technology
Supercond. Sci. Technol. **36** (2023) 105009 (16pp)
https://doi.org/10.1088/1361-6668/acf001

Performance of high-temperature superconducting REBCO coated conductors under synchrotron irradiation for future circular colliders

Patrick Krkotić[1,2,*], Oriol Traver[1], Nikki Tagdulang[1,2], Sergio Calatroni[3], Juan Manuel O'Callaghan[2] and Montse Pont[1,*]

[1] ALBA Synchrotron Light Source, Carrer de la Llum 2-26, 08290 Cerdanyola del Vallès, Barcelona, Spain
[2] UPC-CommSensLab, Department of Signal Theory and Communications, Universitat Politècnica de Catalunya (UPC), c/ Jordi Girona 1, 08034 Barcelona, Spain
[3] CERN, Espl. des Particules 1, Meyrin 1217, Switzerland

E-mail: patrickkrkotic@outlook.de and pont@cells.es

Received 28 April 2023, revised 20 July 2023
Accepted for publication 14 August 2023
Published 29 August 2023

Abstract

The influence of medium-to-high energy synchrotron radiation (SR) (≈10–100 keV) produced by the ALBA Synchrotron Light Source on state-of-the-art REBCO coated conductors (CCs) has been studied to assess the feasibility of using high-temperature superconductors for the beam screen of future circular colliders. Long-term irradiation studies were conducted with *ex-situ* surface resistance testing by using a dielectric resonator. In addition, a cryogenic test system was established for *in-situ* measurements of the critical temperature and surface impedance of REBCO-CCs during synchrotron irradiation, with intensities similar to or above those generated by proton beams circulating in the vacuum chamber in the future circular collider hadron–hadron design. It is shown that the SR impact does not introduce any macroscopic defects that permanently alter the critical temperature or surface impedance of REBCO-CCs. However, the most significant effect of SR is a transient increase in the REBCO's surface impedance. This effect is likely caused by heat, as the material returns to its original impedance values once the radiation exposure stops. The correlation between the time structure of the SR and the possibility of suppressing the Cooper pairing mechanism is also discussed.

Supplementary material for this article is available online

Keywords: REBCO coated conductors, future circular colliders, high-temperature superconductors, surface impedance, synchrotron radiation, critical temperature

(Some figures may appear in colour only in the online journal)

* Authors to whom any correspondence should be addressed.

1. Introduction

Conceptual design studies are currently underway to explore new frontiers of particle physics by expanding the collision energies in the next generation of particle colliders. One of the ongoing feasibility studies is the design of the future circular collider hadron–hadron design (FCC-hh) [1], which aims to succeed the Large Hadron Collider (LHC) [2] as an international collaboration hosted by CERN. The FCC-hh is envisioned as a 100 km long accelerator with a centre-of-mass (cms) collision energy of 100 TeV. Additionally, China, led by IHEP and CAS, has proposed a similar project called the Super Proton–Proton Collider (SPPC), featuring a similar circumference and cms collision energy of 75 TeV [3]. Furthermore, there are plans to upgrade the LHC to a high-luminosity version (HL-LHC) [4], and it may also be further upgraded to a high-energy (HE-LHC) version, with cms energies up to 27 TeV [5].

Future colliders' beam screens will have to cope with unprecedented levels of SR while simultaneously dealing with tighter magnet apertures. The high proton energy in these future colliders will require high magnetic fields to steer the protons, leading to an increase in the emitted synchrotron radiation (SR) compared to any present proton accelerator. For example, in the case of the FCC-hh, superconducting bending magnets (BMs) up to 16 T will be needed to steer the two counterrotating proton beams. The resulting SR originating from these BMs increases by approximately a factor of 160 compared to the LHC, reaching a linear power density of around 35.7 W m^{-1} per beam [6]. In the SPPC, the SR power hitting the inner surface of the beam screen is expected to be 12.8 W m^{-1} [7]. In order to deal with the heat load and cryogenic power needed, the operating beam screen temperature will be set between 40–60 K at the FCC-hh and HE-LHC [1, 5] and 80–100 K at the SPPC [3], compared to the present 5–20 K in the LHC [2]. The higher beam screen temperature used in these colliders will lead to an increase in the electrical resistivity of the materials facing the proton bunches. Additionally, the tighter magnetic aperture will contribute to an increase in what is known as resistive wall impedance. This combined effect can push the resistive wall impedance to a point where the stable operation of the particle beam cannot be guaranteed.

Previous studies [8–13] have provided both theoretical and experimental evidence supporting the use of $REBa_2Cu_3O_{7-x}$ (REBCO, RE = Y, Gd, Eu) high-temperature superconducting coated conductors (CC) in combination with copper as a viable option for a hybrid beam screen material. These studies have directly measured multiple commercially available REBCO-CCs under conditions similar to or matching those found in the FCC-hh in terms of temperature and magnetic field. The results of these studies have demonstrated that REBCO-CCs can exhibit a lower surface impedance compared to copper. However, it should be noted that the impact of SR on the superconducting properties of REBCO-CCs has not yet been determined. As a result, the full feasibility of REBCO-CCs as a beam screen coating cannot be confirmed until this aspect is thoroughly investigated.

There are studies in the scientific literature that use SR-based techniques to gain knowledge on the electronic structure of high-temperature superconductors (HTSs) and possible Cooper pairbreaking mechanisms [14–16]. In contrast, we are unaware of studies that have focused on the effect of SR on the superconducting properties of REBCO-CCs, namely critical temperature and surface impedance, at the functional level. The significance of the critical temperature lies in its correlation and impact on other important superconducting parameters. The greater the difference between the critical temperature and the operational temperature of the accelerator, the more favourable its use will be. Additionally, greater stability in the superconducting parameters facilitates easier operation and prediction of material behaviour. The main reason for considering REBCO-CCs as a substitute material for the beam screen is their ability to substantially decrease the resistive wall impedance, especially at lower frequencies, thanks to their lower surface impedance compared to copper. Whether REBCO-CCs can be used as a coating for the beam screen in a future circular collider largely depends on any alterations in the surface impedance when subjected to SR. Furthermore, this study holds broader significance and can be extended to other applications where strong magnetic fields and high-energy photons are combined, such as in the case of HTS magnets used in fusion applications.

The objective of this study is to analyse the impact of medium-to-high-energy (≈10 keV–100 keV) SR provided by the ALBA Synchrotron Light Source (ALBA) on commercially available REBCO-CCs, summarised in table 1, to understand its usability as a potential beam screen coating in a future particle collider. This paper is divided into seven sections. Section 2 includes a brief review of the relevant concepts of SR in the FCC-hh beam screen. Section 3 describes the experiments to assess the possible degradation of REBCO-CCs subjected to long-term irradiation exposure to high-energy photons. Sections 4 and 5 address the *in-situ* medium-to-high energy photon impact on the superconductors' characteristics of critical temperature and surface impedance, respectively. The findings of the measurements are discussed and evaluated in detail in section 6. Section 7 deals with the conclusions.

2. SR at FCC-hh versus ALBA

Synchroton radiation refers to the electromagnetic radiation emitted by charged particles that are accelerated to relativistic speeds passing through a magnetic field. The SR is emitted tangentially from any point along a curved path followed by the charged particle in a highly collimated forward direction with a vertical opening angle $1/\gamma$, where γ refers to the Lorentz gamma factor [18]. The radiation is emitted in a broad energy spectrum determined by the particle rest mass, the beam energy E_{beam}, and the bending radius R_{BM} of the magnet, or equivalently the magnetic field B_{BM}. As an illustration, figure 1 shows the spectral photon flux as a function of photon energy for the ALBA Synchrotron compared to that in the FCC-hh. The same figure shows that the photon flux in the

Table 1. REBCO coated conductor architecture and critical temperature for various providers [9, 10, 17].

	Bruker	Fujikura	SuNAM	SuperOx	SuperPower	Theva
Rare-earth	Y	Gd	Gd	Gd	{Y,Gd}	Gd
Thickness (μm)	1.6	1.8	1.6	0.9	1.5	3.0
Nano-inclusion	$BaZrO_3$	none	none	none	$BaZrO_3$	none
Substrate	Stainless Steel	Hastelloy C276	Hastelloy C276	Hastelloy C276	Hastelloy C276	Hastelloy C276
Thickness (μm)	100	75	100	60	50	100
T_C (K)	85	94	94	94	91	92

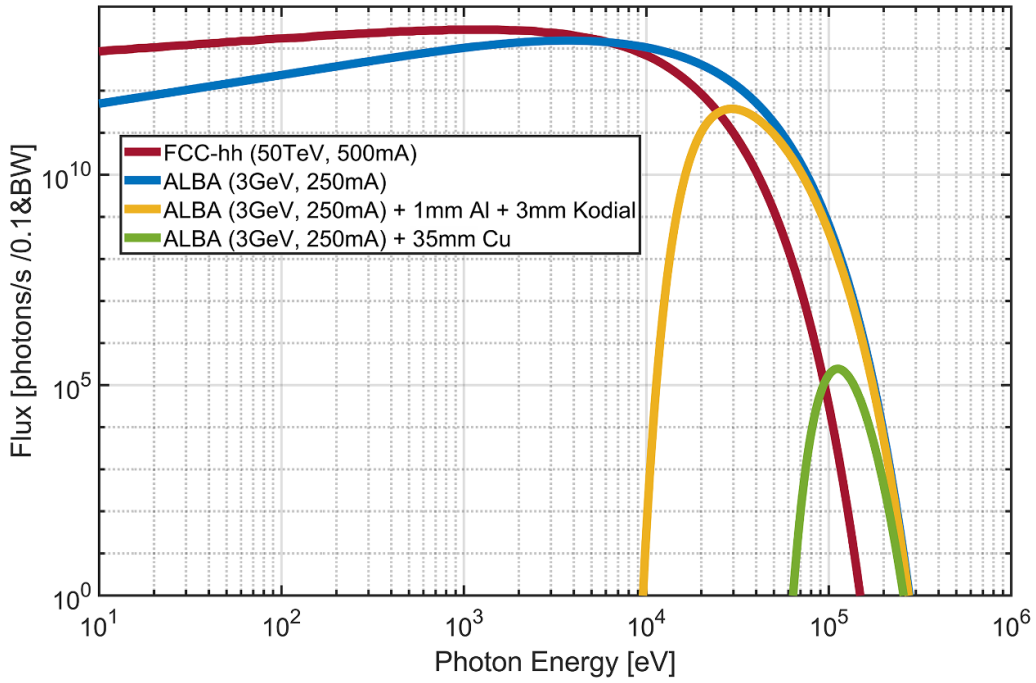

Figure 1. Synchrotron radiation flux spectra comparison between FCC-hh and ALBA. The yellow and green lines show particular configurations of the experiments that will be mentioned later in the text.

FCC-hh is comparable to ALBA's. This is a consequence of ALBA accelerating electrons, which are lighter than the protons accelerated at the FCC-hh.

In the case of electrons, the total power per beam P_{tot} and the linear power density P_{lin} can be estimated as [19]:

$$P_{\text{tot}}[\text{W}] = 2.65 \cdot 10^4 \, E^3_{\text{beam}}[\text{GeV}] \, B_{\text{BM}}[\text{T}] \, I_{\text{beam}}[\text{A}], \quad (1)$$

$$P_{\text{lin}}[\text{W mradH}^{-1}] = 4.22 \, E^3_{\text{beam}}[\text{GeV}] \, B_{\text{BM}}[\text{T}] \, I_{\text{beam}}[\text{A}], \quad (2)$$

where I_{beam} is the beam current. Note that linear power, measured in W mradH^{-1}, refers to the power emitted by an electron beam in an angular opening of 1 mrad in the horizontal plane. For protons, the results have to be scaled by a mass-ratio-factor of an electron to proton $a_{\text{e-p}} = 1/1823$ to calculate the appropriate power [19]. Table 2 summarises the characteristic values of these two accelerators and the estimated power values, showing that the total and linear power between ALBA and FCC-hh differ only by approximately a factor of 10. In this paper, SR will be quantified by the beam current responsible for generating the SR. As shown in equations (1) and (2), the SR power is directly proportional to the beam current when the other parameters are kept constant, as is the case in the ALBA storage ring. Furthermore, in the case of ALBA, the beam current is always to be understood as electron beam current.

Table 2. Synchrotron radiation power estimations for ALBA (electron accelerator) and FCC-hh (proton accelerator) based on each accelerators' specific parameters.

	E_{beam} (GeV)	I_{beam} (mA)	B_{BM} (T)	P_{tot} (kW)	P_{lin} (W mradH^{-1})
ALBA	3	250	1.42	254	40
FCC-hh	50 000	500	15.96	2400	382

ALBA has short magnets with a small radius of curvature. In this respect, the unused SR can be stopped at lump absorbers, the so-called crotch absorbers, which are water-cooled bulk copper blocks that absorb all but the most energetic photons above 80 keV. In the FCC-hh with much longer magnets $\approx$14 m [1] with a much larger bending radius, SR must be absorbed inside the magnets. To minimise photon-induced effects on the proton beam, the beam screens of the FCC-hh consist of two concentric structures. The outer beam screen, designed to meet various technical specifications, serves the purpose of separating the cold bore of the

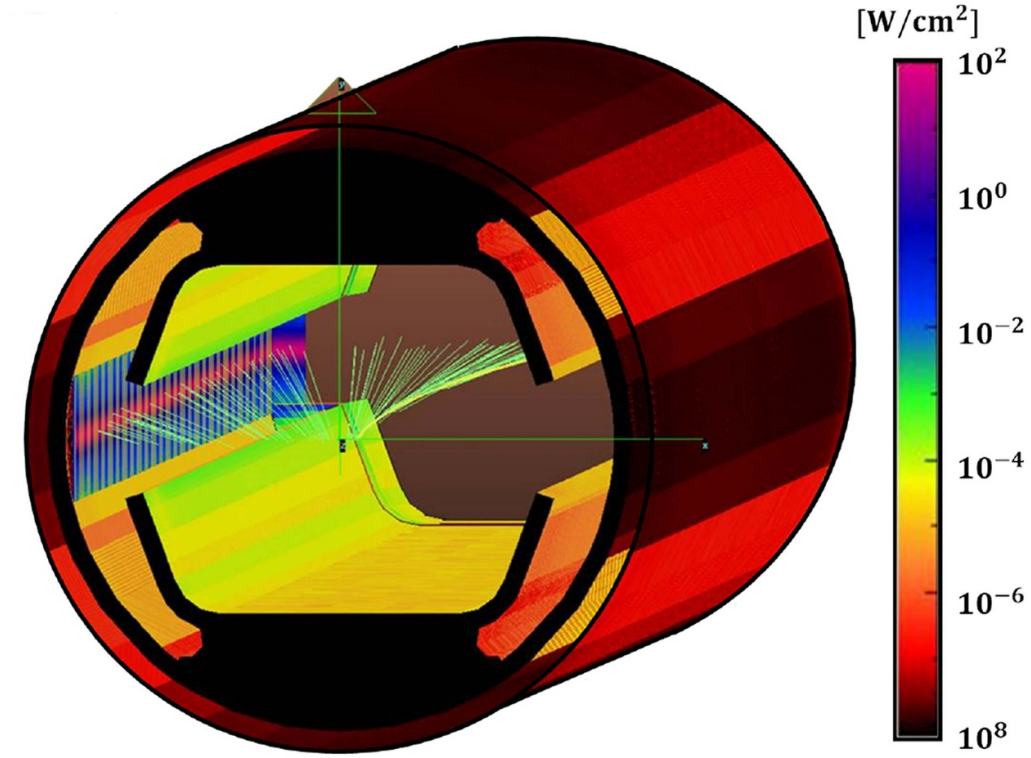

Figure 2. Power density of the SR deposited in the 15 m FCC-hh beam screen.

magnets from the beam and absorbing the SR emitted by the proton beam. The inner beam screen, on the other hand, should ensure the removal of the resistive losses dissipated by the wall currents induced by the proton beam. Figure 2 shows the SR power deposited on the beam screen of the FCC-hh. The yellow curved line in the centre depicts the particle beam trajectory. The green fan-like lines indicate the SR emitted tangentially to the trajectory in a very narrow vertical aperture. Most of the SR will be absorbed on the outer beam screen, thanks to the 7.5 mm slot of the inner chamber [20]. Still, a small portion of the SR will reach the inner chamber directly or indirectly (due to reflections), where the REBCO-CCs are considered to be positioned. With the help of SYNRAD+ [21], a photon ray tracing program that takes into account the photon reflections, the total power deposited on the 15 m beam screen of a dipole magnet is estimated to be $P_{\mathrm{BS}} = 0.6\,\mathrm{W}$ with a maximum surface power density of $p_{\mathrm{BS}} = 0.3\,\mathrm{mW\,cm^{-2}}$, in accordance with previously simulated values [20].

3. *Ex-situ* SR impact on the surface resistance

Since the beam screen at the FCC-hh will be constantly irradiated by SR, it is also of interest to determine whether the REBCO-CCs lose their superconducting characteristics after long-term exposure to SR. A study was performed by placing samples from different providers behind various ALBA crotch absorbers during approximately 550 h, comparing the surface resistance R_S of the samples before and after irradiation.

3.1. *Experimental arrangement for* ex-situ *testing*

Samples were obtained from five different providers available at the time of the experiment. These samples, which had varying CC architectures, were cut into square pieces measuring 12 mm × 12 mm. They were then positioned behind the ALBA crotch absorbers, where the samples were exposed to SR at a normal incidence angle. A schematic representation of the experimental arrangement is shown in figure 3, illustrating the BM where the SR is generated and the proximity to the crotch absorber where a pair of REBCO samples are positioned. The vacuum chamber between the BM and the crotch absorber is removed to visualise the photon flux. The crotch absorbers at ALBA are made of copper with 35 mm thickness, and as a consequence, SR is strongly absorbed; thus, only a low-intensity photon flux of energies above $E_\gamma > 80\,\mathrm{keV}$ can go through to impinge on the samples. The remaining photon flux reaching the samples is shown as a solid green line in figure 1.

The experiment was performed twice, once with a beam current of $I_{\mathrm{beam}} = 150\,\mathrm{mA}$ and once with $I_{\mathrm{beam}} = 250\,\mathrm{mA}$. In both experiments, the samples were continuously exposed to SR for about 550 h, equivalently to about one month of operation. The deposited flux at the surface of each sample after the crotch absorbers is for all samples the same and equals $F_{\mathrm{dep}} = 5.3 \cdot 10^7\,\mathrm{ph\,s^{-1}\,mradH^{-1}}$ at a beam current of $I_{\mathrm{beam}} = 150\,\mathrm{mA}$. Considering the above-mentioned total irradiation time and the experimental geometry, this leads to a total amount of $F_{\mathrm{dep}} = 6.3 \cdot 10^{14}$ photons, which translates into a total deposited power of $P_{\mathrm{dep}} = 51\,\mathrm{nW}$ per sample. A density of about

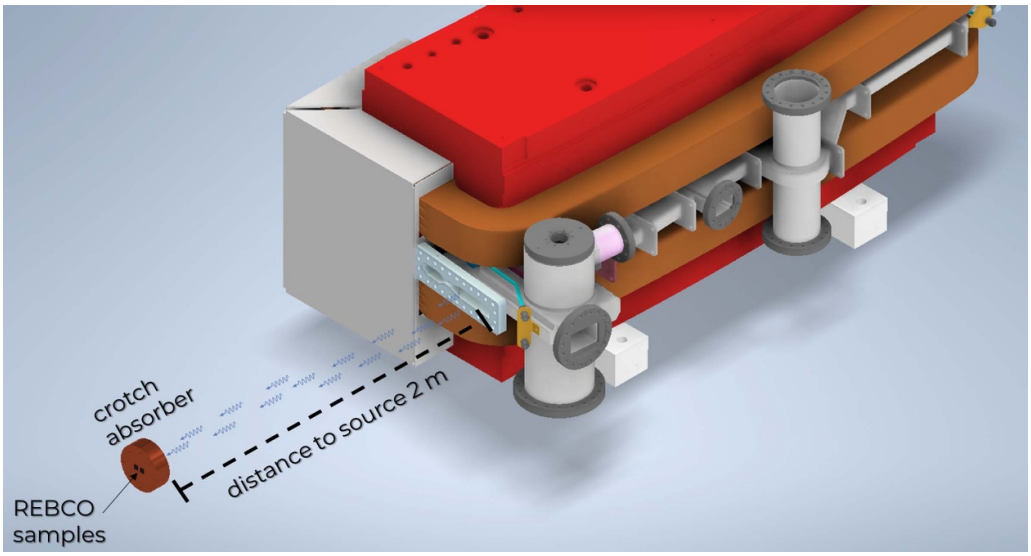

Figure 3. Experimental set-up for *ex-situ* REBCO-CC sample irradiation at the ALBA synchrotron.

Table 3. Radiation key parameters of the ALBA Synchrotron long term irradiation experiment. $I_{beam} = 150$ mA The parameters at a beam current of $I_{beam} = 250$ mA can be determined by multiplying all given values by a factor of 1.7.

	d (μm)	F_{abs} 10^{11} (ph)	P_{abs} (pW)	E_{abs} (μJ)	Dose (Gy)
Bruker	1.6	3.1	25	49	393
SuNAM	1.6	3.1	25	49	393
SuperOx	1.5	1.7	14	28	393
SuperPower	0.9	2.9	23	46	392
Theva	3.0	5.7	46	92	392

$\rho_{density} = 6.3\,g\,cm^{-3}$ [22] has been assumed for the REBCO, excluding buffer layers and stabilisers. Due to differences in the thickness d of the REBCO layer among the different providers, the total absorbed flux F_{abs}, energy E_{abs}, and power P_{abs} differ from sample to sample. Irradiation of the sample was controlled by attaching the REBCO-CCs onto green photosensitive dosimetry film by GAFChromic™. The samples were exposed to a dose of approximately 400 Gy. Furthermore, to assess whether any observed degradation is solely caused by SR or if exposure to air could also contribute, control samples were stored in the storage ring tunnel without undergoing irradiation. New samples were prepared for each experiment. The cumulative radiation parameters for each provider are presented in table 3, and the methodology for determining these values is provided in the supplementary information A.

Throughout this paper, we will refer to a REBCO-CC as the REBCO attached to buffer layers and a substrate. When mentioning the REBCO layer, solely the REBCO component is to be understood.

3.2. Ex-situ *measurements and results*

Possible degradation of the superconducting properties of the REBCO-CCs has been examined by measuring the surface resistance R_S of the samples and comparing the results before and after irradiation. The measurement method selected for these experiments is based on a Hakki-Coleman dielectric resonator (DR) [23] following the work by Klein *et al* [24], who used titanium dioxide (rutile) for the characterisation of high-temperature superconductors on account of its very low dielectric losses and high permittivity. The general design consists of a metallic cylinder loaded with a high-permittivity and low-loss dielectric material and shielded by a pair of samples to be analysed. The design and functioning of the DR in this study, which is discussed in detail in the supplementary information B, has been adapted specifically to the dimensions of the samples to perform measurements at low temperatures and under DC magnetic fields [25]. This method has been shown to measure surface resistances over a wide range of materials with high precision and reproducibility [9, 26–28].

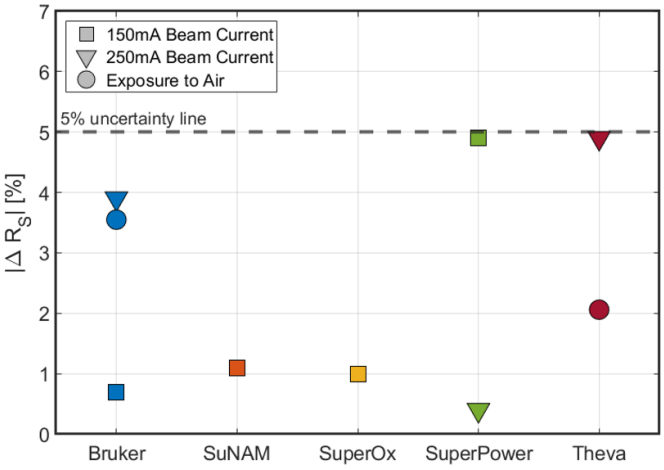

Figure 4. Absolute changes in surface resistance at 77 K, after 550 h of irradiation with photon energies $E_\gamma > 80$ keV.

Figure 4 presents the measured absolute changes in surface resistance $|\Delta R_S|$ for different manufacturers before and after

being exposed to SR generated by the 150 mA and 250 mA beam currents in the ALBA storage ring. Each data point represents an individual irradiated sample pair, and no comparison is made to other sample pairs of the same provider. In addition, we include in the graph a 5% line indicating the uncertainty of the measurements with the given DR [26] as well as the results for the non-irradiated control samples. As seen in figure 4, changes in $|\Delta R_S|$ are within the measurement uncertainty irrespective of the condition to which the samples were subjected.

4. *In-situ* SR impact on the transition temperature

Since the REBCO-CCs in the beam screen of the FCC-hh will be irradiated while being in the superconducting state, it is of high importance to understand the behaviour of REBCO-CCs' superconducting characteristics during the operation of the accelerator. Hence, the first *in-situ* study was performed with DC transport measurements to examine the behaviour of the critical temperature T_C and critical temperature transition width ΔT_C of REBCO-CC samples before and after irradiation.

Various changes in the superconducting properties may be induced by SR and detected while measuring the critical temperature. One possible change is a non-reversible shift in T_C, indicating permanent damage to the superconductor, which can result from factors like a change in oxygen stoichiometry, known to affect the critical temperature of REBCO [29]. Another possibility, rather than permanent sample damage, is the suppression of the superconducting state during irradiation due to photon-induced breaking of Cooper pairs (CP) [14, 15]. In this case, an expected outcome is the broadening of the critical temperature transition width (ΔT_C) compared to measurements without irradiation. Especially, when considering the two-fluid model [30], near the critical temperature, the number of CP becomes significantly reduced. Furthermore, in the case that in the central part of the sample, where the SR power density is maximum, the superconductivity should be locally suppressed and the material transitions locally into the normal conducting state, a higher resistance would be measured below T_C.

4.1. *Experimental arrangement for* in-situ *testing*

In order to determine the effect of SR on REBCO-CCs *in-situ*, a cryogenic measurement set-up was implemented within the ALBA particle accelerator infrastructure diagnostic beamline inside the accelerator tunnel. It is important to note that the experimental set-up was not accessible during normal operation for the accelerator users. This limitation significantly restricted the time available for conducting experiments and the number of samples that could be tested. At this location, SR with a horizontal opening of 1 mrad reaches the REBCO-CC sample placed inside a cryostat, as presented in figure 5. The cryostat is situated 14 m from the source and the SR footprint is $16 \times 5\,\mathrm{mm}^2$ (horizontal $\times$ vertical). Between the BM and the cryostat, the photons pass through an aluminium window of 1 mm thickness, which separates the accelerator vacuum from atmospheric pressure, and also a 3 mm thick Kodial-glass viewport, which separates room temperature from cryogenic temperatures at the cryostat. Consequently, the photon flux is reduced to medium-to-high-energy photons, $E_\gamma > 10\,\mathrm{keV}$, as shown in figure 1 with the solid yellow line.

The measurements have been performed with a continuous flow cryostat (Janis Research Model ST-400 UHV Supertran System) that can operate between $T = 4$ and 350 K. As shown in the cross-sectional view of the cryostat in figure 6, the Supertran System contains a cold finger equipped with an internal heater and a temperature sensor to control the temperature. At the end of the cold finger, there is a gold-plated copper sample holder measuring 14 mm $\times$ 13 mm. The REBCO-CC samples can be mounted and wired on this holder, as depicted in the enlarged view shown in the inset of figure 6.

Figure 7 provides a sketch of a 5 mm $\times$ 12 mm sample to measure the critical temperature mounted on the cold finger. The REBCO-CC sample was photolithography patterned to enable the measurement of the resistance as a function of temperature in a four-wire configuration. The pattern consists of a 1 mm $\times$ 10 mm long superconducting strip with a pair of side pads at both ends. These side pads serve a dual purpose: they allow the passage of a $I = 1$ mA direct current and enable the simultaneous measurement of voltage. The current and voltage pads are made of the pre-existing silver layer, whose initial function is to protect the REBCO layer inside the CC configuration. High-conducting silver paint was used to attach silver wires to the superconductor. In this configuration, as shown in figure 7, the SR hits the superconducting stripe in the centre. An additional temperature sensor (Cernox CX-1050-SD-HT) has been installed next to the sample for additional temperature monitoring. The irradiation of the sample during the operation of the accelerator is indicated in two ways; by the photosensitive dosimetry film being placed at the position of the cryostat Kodial window and by a possible rise in temperature.

For this investigation, a beam current I_{beam} of either 100 mA or 200 mA was used to irradiate the samples with photons. The critical temperature under irradiation has been measured for two providers: SuperPower ($T_C = 91$ K), which contains artificial pinning centres (APCs) and SuperOx ($T_C = 92$ K), a pristine sample whose microstructure relies on an as-grown pinning landscape with twin boundaries, stacking faults, and point defects [9, 10]. The reason for selecting these two samples was to conduct measurements on one REBCO-CC sample with APCs and one pristine sample. The irradiation exposure period per experiment was about 2 h and resulted in a total amount of photons of $F_{\mathrm{dep}} = 1.5 \cdot 10^{18}$ with a deposited power of $P_{\mathrm{dep}} = 33\,\mathrm{mW}$ impinging on the REBCO layer surface. The samples were exposed to a dose of 46 kGy. The duration of the experiment is given by the rate of change of the temperature. Table 4 summarises the characteristic radiation parameters for each provider. The calculation methodology for these values is detailed in the supplementary information C.

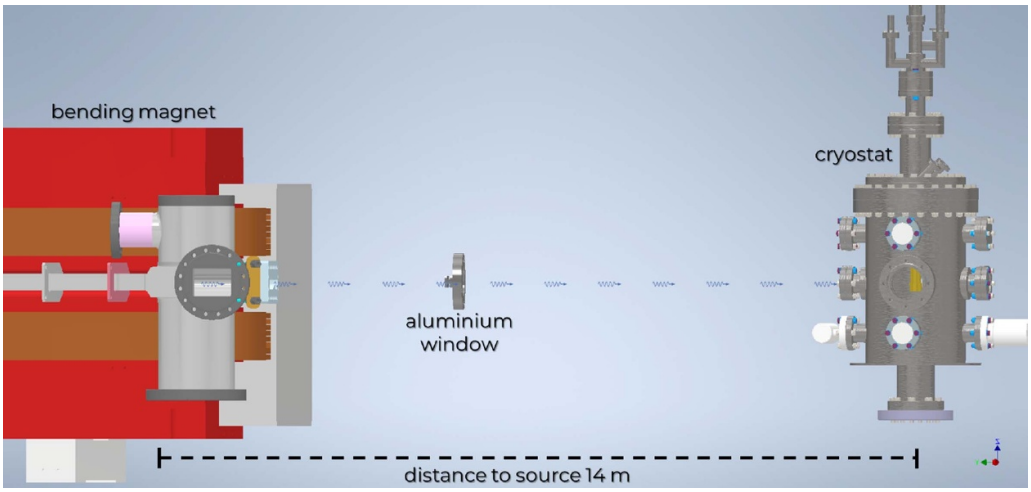

Figure 5. Experimental set-up for *in-situ* irradiation measurements of the critical temperature and the surface resistance under SR at the ALBA synchrotron.

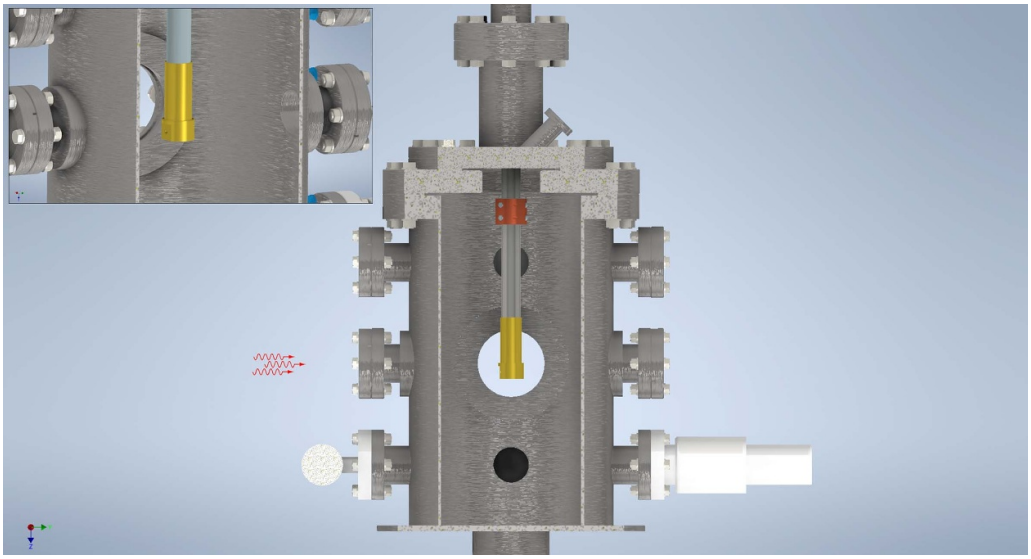

Figure 6. Cross-sectional view of the cryostat, including an enlarged view of the cold finger and its sample holder.

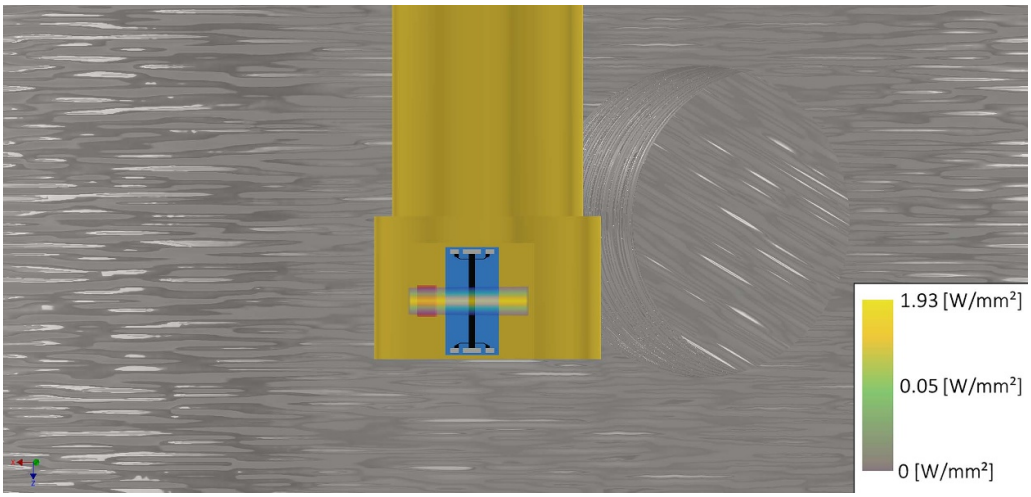

Figure 7. Cold finger sample holder with a patterned REBCO-CC sample mounted for T_C-measurements under SR. The additional temperature sensor is shown in orange as well as the SR power density distribution.

Table 4. Radiation key parameters of the *in-situ* ALBA Synchrotron T_C measurement experiment for $I_{\text{beam}} = 100$ mA. The parameters at a beam current of $I_{\text{beam}} = 200$ mA can be determined by multiplying all given values by a factor of 2.

	d (μm)	F_{abs} 10^{15} (ph)	P_{abs} (mW)	E_{abs} (J)	Dose (kGy)
SuperOx	0.9	8.3	0.3	1.3	46
SuperPower	1.5	13.7	0.3	2.2	46

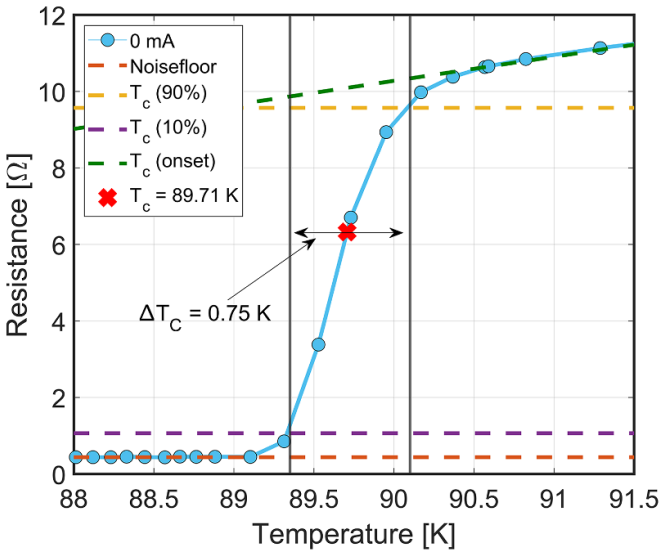

Figure 8. Example of the determination of T_C with SuperPower.

4.2. *Critical temperature measurements*

The temperature of the samples was first stabilised at 85 K, well below the expected critical temperature. Afterwards, the resistance R was recorded approximately every 150 mK while slowly raising the temperature at a rate of 0.5 K min^{-1} until the critical temperature was reached. Measurements of T_C without SR ($I_{\text{beam}} = 0$ mA) were taken before and after irradiation to be used as reference.

Figure 8 shows how the the critical temperature and critical temperature transition width was determined. First, the temperature range in which the measurement signal drops from 90% to 10% of the step height is identified, simultaneously defining ΔT_C. The critical temperature is the temperature at 50% of the critical temperature transition width. In this particular example for SuperPower, the critical temperature value was measured at $T_C \approx 90$ K, close to the expected value of $T_C \approx 91$ K.

Prior to commencing the study, the accuracy of the set-up was tested by repeating four measurements of T_C of the same sample without irradiation. The mean uncertainty in the critical temperature between measurements is obtained by comparing the resistance versus temperature (R–T) curves normalised to the T_C estimated for the first temperature cycle. The mean uncertainty results in $\Delta T = \pm 0.0002 \cdot T_C \approx \pm 20$ mK, which is slightly higher than the accuracy of the attached Cernox temperature sensor $\approx \pm 10$ mK [31].

Figure 9 presents the measured resistances as a function of the normalised temperature for both providers. Each $R-T$ curve has been normalised based on the measured T_C for that particular measurement. Additionally, the insets show an enhanced view of the measured $R-T$ data, including the expected uncertainties. As can be seen in both insets, the various $R-T$ curves overlap within the expected temperature uncertainty. Accordingly, the results for both REBCO-CC providers indicated neither a change in the transition width nor any change in the critical temperature or enhanced resistance below T_C.

5. *In-situ* SR impact on the surface impedance

The primary motivation for considering REBCO-CCs as an alternative beam screen material is their potential to significantly reduce the resistive wall impedance, particularly at low frequencies, due to their lower surface impedance compared to copper [9–11]. The viability of using REBCO-CCs as a beam screen coating for a future circular collider heavily depends on any changes in the surface impedance Z_S when exposed to SR. Unlike in DC transport measurements/properties, the presence of non-superconducting quasiparticles affects the radio frequency (RF) surface impedance. A higher amount of quasiparticles leads to a higher surface impedance. Thus, it is of fundamental importance for this study to determine if the REBCO-CC retains its reduced surface impedance compared to copper, even when exposed to impinging photons. Besides, these data can also be used to derive secondary information regarding the placement options inside a beam screen.

5.1. *Experimental arrangement for* in-situ *testing*

To assess if the surface impedance is affected by SR, a parallel-plate resonator (PPR) compatible with the cryostat described in section 4.1 was designed. In addition, the dimensions of the PPR were optimised to operate close to a resonance frequency of $f_0 \approx 1$ GHz, which is within the power frequency spectrum of all future hadron colliders [1, 3, 5]. Figure 10 depicts a cross-sectional view of the cryostat, modified to accommodate the PPR. As can be seen, the cold finger was elongated by a copper fixture base to hold and ensure proper thermal anchoring of the PPR.

The PPR pioneered by Taber [32] is a DR which uses a dielectric with a very high aspect ratio separating two samples to be examined. The PPR in this experiment, as sketched in more detail in figure 11(a), is formed by two parallel REBCO layers, one on top of the other and separated by a thin dielectric layer made out of a single crystal c-axis sapphire with the dimensions of $54 \times 12 \times 0.25$ mm. To ensure mechanical stability and adequate holding of the samples, one REBCO-CC is affixed to a copper plate using thermal paste and attached to the sample holder on the cold finger. On the other side of the sapphire, a delaminated [12, 33] REBCO-CC is glued to the fixture base, also using thermal paste. Two providers have been used for this study: SuperPower ($T_C = 91$ K) and Fujikura ($T_C = 94$ K). The reason for selecting these two samples was

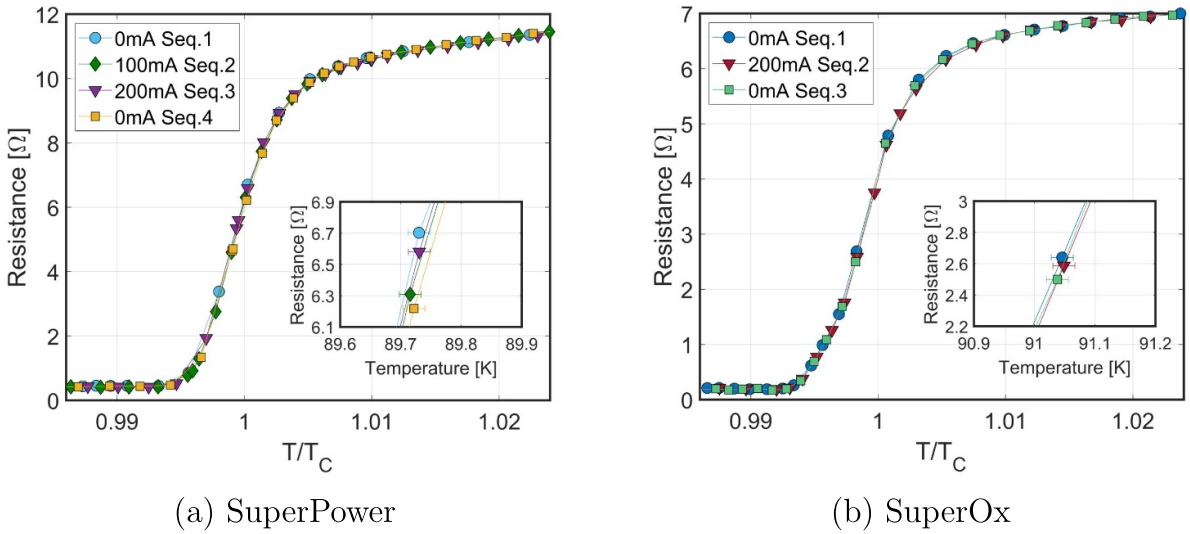

Figure 9. Critical temperature measurements for SuperPower and SuperOx under SR, compared to the non-irradiation reference.

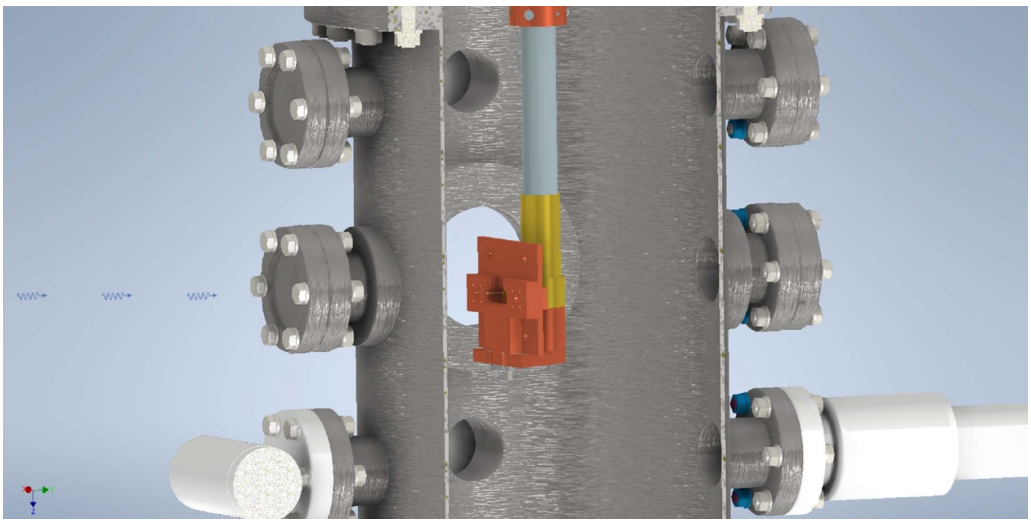

Figure 10. View of the PPR inside the cryostat.

not only to conduct measurements on one REBCO-CC sample with APCs and one pristine sample but also due to the possibility of clean delamination of the REBCO materials with these two specific providers. The delamination process [34] is a complex process that depends strongly on the buffer layers and the stabilisers. These two providers were chosen because they provide the best quality of delaminated samples. Furthermore, the previous measurements conducted for all providers demonstrated the lowest surface resistance values for REBCO-CCs provided by these manufacturers [9–11]. Consequently, we anticipated the highest quality factor values for the PPR using the REBCO-CCs provided by these suppliers. This advantage translates into a better signal-to-noise ratio and cleaner resonance curves. An oval cut-out machined on the fixture base assures irradiation of the samples without additional absorption other than the Al and the Kodial windows already mentioned, albeit at the expense of possibly losing good adhesion between the delaminated conductor and the fixture base with the cut-out. In the PPR, the surface currents flow longitudinally along the length of the REBCO-CC tapes, with the maximum current coinciding with the maximum SR power density for well-aligned samples. Figure 11(b) shows the front view of the PPR with the SR intensity profile superimposed. Further details about the PPR are given in the supplementary information D. It should be noted that the key radiation parameter values in this experiment, as summarised in table 5, change significantly, despite the sample's position and the irradiation time being the same as in the critical temperature measurements in section 4. This is due to the larger irradiation area compared to the measurements of the critical temperature. The incoming flux at the sample's surface is the same for all samples and equals $F_{\mathrm{dep}} = 3 \cdot 10^{15}\ \mathrm{ph\,s^{-1}\,mradH^{-1}}$ at a beam current of $I_{\mathrm{beam}} = 100\ \mathrm{mA}$. The average exposure period for each experiment is roughly two hours, resulting in a total amount of photons of $F_{\mathrm{dep,total}} = 2.2 \cdot 10^{19}$ impinging on the delaminated REBCO layer surface. As a consequence, a power

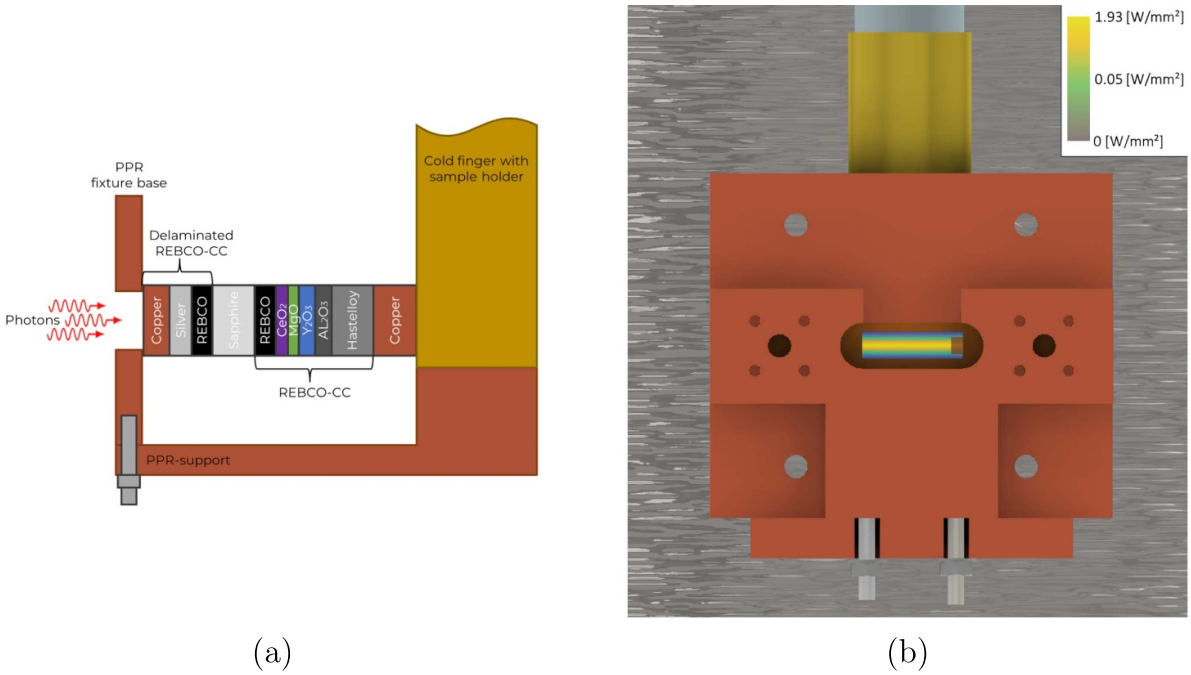

Figure 11. Experimental arrangement of the PPR: (a) layered structure of the two samples on the PPR (the scale is exaggerated), (b) front view of the PPR with the SR profile superimposed.

Table 5. Radiation key parameters of the *in-situ* ALBA Synchrotron R_S measurement experiment at a beam current of $I_{\text{beam}} = 100\,\text{mA}$. The parameters at a beam current of $I_{\text{beam}} = 250\,\text{mA}$ can be determined by multiplying all given values by a factor of 2.5.

	d (μm)	F_{abs} 10^{17} (ph)	P_{abs} (mW)	E_{abs} (J)	Dose (kGy)
SuperPower	1.5	2.0	4.3	31	42
Fujikura	1.8	2.3	5.2	37	42

of $P_{\text{dep}} = 0.5\,\text{W}$ is deposited on the delaminated CC REBCO layer. The samples were exposed to a dose of 42 kGy. The supplementary information C provides details on how these values were obtained.

5.2. Temperature sweep at constant beam current

This section presents the results of the *in-situ* irradiation dependence of the complex surface impedance $Z_S = R_S + iX_S$ with temperature, where R_S and X_S refer to the surface resistance and reactance, respectively. First, the samples were cooled down and stabilised at $T = 40\,\text{K}$. Then, while being irradiated with SR from a beam current of $I_{\text{beam}} = 100\,\text{mA}$, data was collected approximately every 300 mK during a temperature rise at a rate of $2\,\text{K}\,\text{min}^{-1}$. For reference, measurements of Z_S without SR ($I_{\text{beam}} = 0\,\text{mA}$) were performed both before and after irradiation. As per the two-fluid model, the surface resistance R_S and surface reactance X_S are influenced by the fraction of CP [35, 36]. Thus, at any given temperature, an increase in R_S observed during irradiation, resulting in a decrease in the unloaded quality factor (Q-factor) Q_0, and the rise in X_S, leading to a lower resonance frequency f_0, can be attributed to the disruption of CP. Further information about these dependencies is explained in the supplementary information D.

The measured Q-factor and resonance frequency as a function of temperature with and without the influence of SR are presented in figure 12. The Q-factor decreases gradually as a function of temperature, with a significant decline at the expected T_C. The results do not, however, reveal any significant difference in the behaviour during and after irradiation with a beam current of $I_{\text{beam}} = 100\,\text{mA}$. The resonance frequency versus temperature exhibits similar behaviour, except for a slight noise pattern present during irradiation.

5.3. Beam current ramp at constant temperature

During the operation of the FCC-hh, the beam screen will be kept at temperatures close to 50 K while the SR impinges continuously on the beam screen surfaces. Furthermore, during injection, the magnetic field will be ramped from injection $B_{\text{BM}} = 1\,\text{T}$ up to collision $B_{\text{BM}} = 16\,\text{T}$, leading to a continuous increase of SR power on the beam screen. Similar to this scenario, the surface impedance was measured as a function of the injected beam current from $I_{\text{beam}} = 0$ to 250 mA while keeping the cold finger at a constant temperature of $T = 50\,\text{K}$. Two different measurement procedures were followed. In the first one, the Q-factor and the resonance frequency were measured while increasing and decreasing the beam current. In the second procedure, the beam was dumped after $I_{\text{beam}} = 250\,\text{mA}$ was reached. This leads to an instantaneous loss of beam, and thus, as well of SR. Both scenarios are common in such high-energy circular colliders.

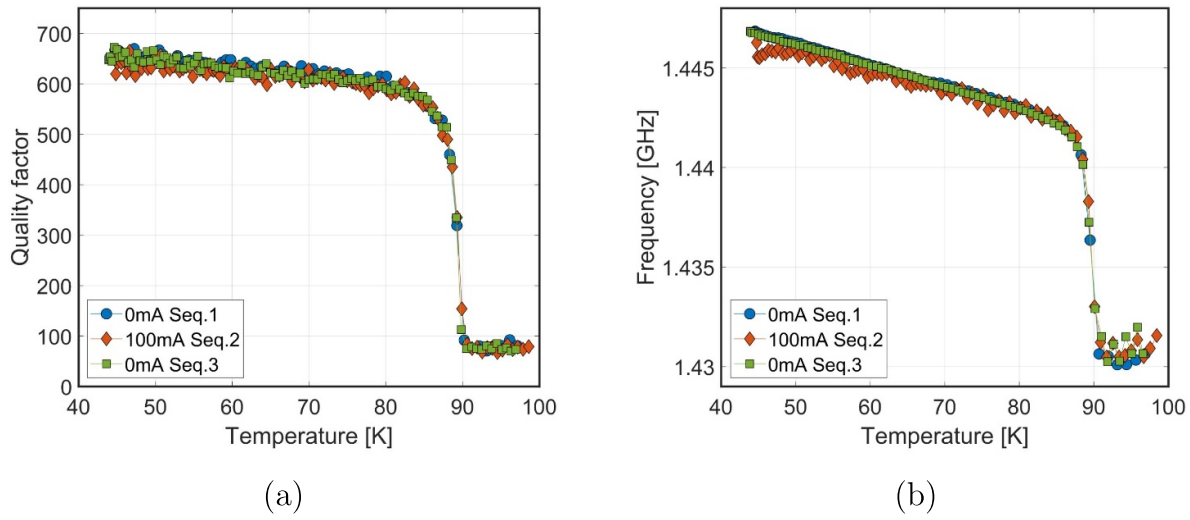

Figure 12. *In-situ* unloaded quality factor and resonance frequency measurement of a REBCO coated conductor from SuperPower with and without synchrotron irradiation.

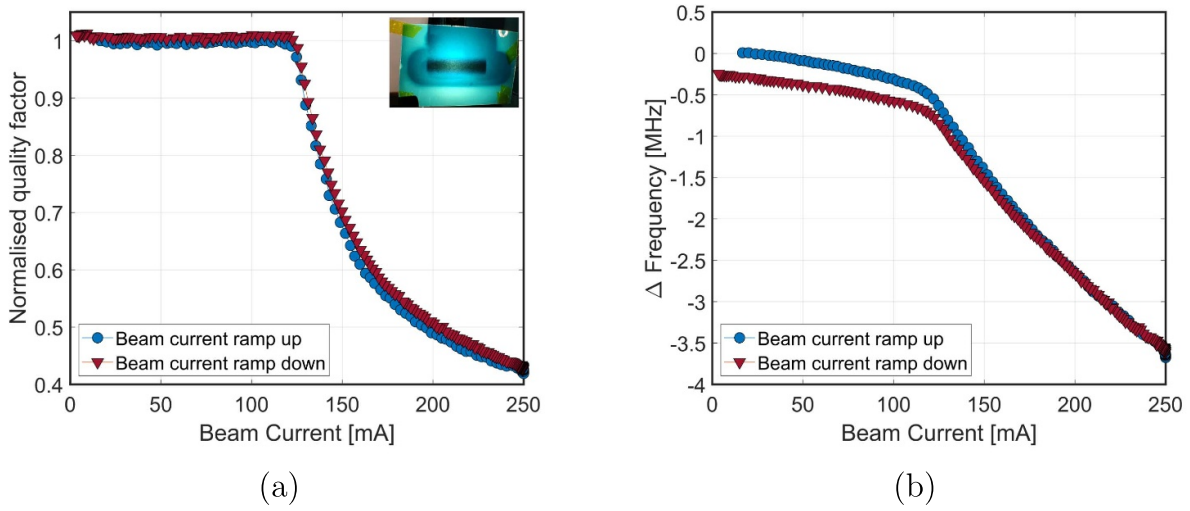

Figure 13. Quality factor and resonance frequency as a function of beam current at 50 K for a Fujikura REBCO-CC. In blue while increasing the beam current up to 250 mA, in red while decreasing the beam current back to 0 mA.

Figure 13 displays (a) the normalised quality factor $Q_{\text{norm}} = Q_i / Q_{I_{\text{beam}=0}}$, where $Q_{I_{\text{beam}=0}}$ refers to the average of the first five quality factors measured at $I_{\text{beam}} = 0$ mA, against the beam current, and (b), the change in resonance frequency $\Delta f_0 = f_{I_{\text{beam}=0}} - f_i$, where $f_{I_{\text{beam}=0}}$ refers to the average of the first five resonance frequencies measured for Fujikura samples at $I_{\text{beam}} = 0$ mA. The blue data points in both subfigures show values while increasing the beam current from $I_{\text{beam}} = 0$ to 250 mA with a filling rate of approximately 30 mA per min. In contrast, the red data points indicate the values measured while lowering the beam current back to zero. As shown in figure 13(a), the normalised Q-factor seems unaffected when ramping the beam current up to about $I_{\text{beam}} \approx 120$ mA. Once the beam current is above 120 mA, the unloaded Q-factor gradually decreases until it reaches a minimum value of 40% of the starting value at $I_{\text{beam}} = 250$ mA. A decrease in the Q-factor of this magnitude indicates that the sample is transitioning into the normal conducting state. Regarding the influence of the dielectric spacer, sapphire losses are known to be very small at cryogenic temperatures. By calculating the necessary change in the sapphire losses in order to achieve a 60% change in Q_{norm}, a loss tangent value close to room temperature is obtained. Hence, it is not possible that changes in Q_{norm} are primarily due to variations in the losses of sapphire. Reducing the beam current reveals that the process is reversible. The normalised Q-factor returns to its initial value, demonstrating that SR has not permanently damaged the sample, consistent with the previous experiments.

The experimental data on the changes in resonance frequency in figure 13(b) reveals the same general behaviour as the Q-factor. Above a beam current of $I_{\text{beam}} = 120$ mA, the change in resonance frequency is steeper. The overall Δf_0 is consistent with the sample or the affected area of the sample transitioning into the normal conducting state during

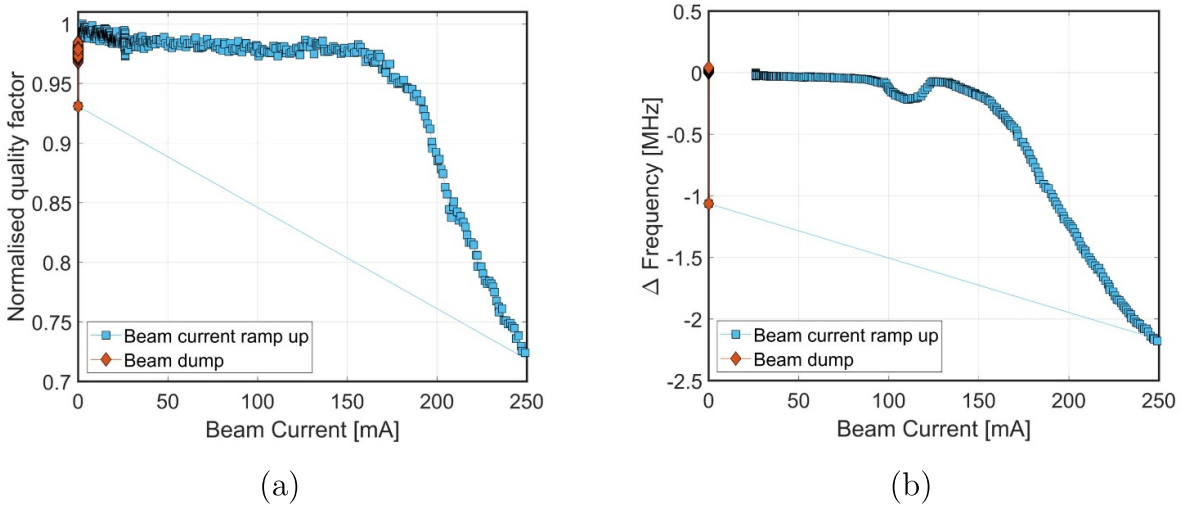

Figure 14. Quality factor and resonance frequency as a function of beam current at 50 K for a SuperPower REBCO-CC, in blue while increasing the beam current up to 250 mA, in orange the data corresponding to the beam dump.

irradiation. However, even though the process is reversible, at low beam currents, the resonance frequency remains lower than the one measured when increasing the current. This cannot be solely due to the heating of the sapphire dielectric during irradiation. Generally, resonance frequency measurements are more sensitive to mechanical and thermal changes than quality factor measurements. Such a decrease in resonance frequency after irradiation of about $\Delta f_0 \approx 250$ kHz while the resonance is at $f_0 \approx 1.2$ GHz can most certainly be explained due to the thermalisation process, and a slight temperature drift connected to the proportional-integral-derivative (PID) controller of the temperature control unit trying to reach the precise demanded set temperature.

The results for SuperPower are shown in figure 14. The Q_{norm} reduces already linearly by 3% up to a beam current of $I_{\text{beam}} \approx 150$ mA before a noticeable decrease down to 70% of the initial value is visible at a maximum beam current of $I_{\text{beam}} \approx 250$ mA. Shortly after reaching the desired beam current (1 min), the beam was dumped, and a rapid recovery of the normalised quality factor can be seen in the data points taken (every 5 s). From the data in figure 14(b), it is apparent that the change in resonance Δf_0, again follows the same behaviour as the Q_{norm}. The cause of the observed bump around 110 mA remains unknown, however, the fact that it is not observed on the quality factor suggests that it might be an artefact of the measurement.

6. Discussion

The findings of section 3 indicate that REBCO-CCs sustain their superconducting properties when exposed to long-term photon irradiation. The *ex-situ* examination, using a non-destructive technique based on a DR, did not detect any evidence of permanent damage on the REBCO-CC layer caused by SR at photon energies $E_\gamma > 80$ keV after 550 h of irradiation. Additionally, the findings from both *in-situ* experiments demonstrated no damage on the samples to significantly alter their superconducting properties in the short term due to SR at photon energies $E_\gamma > 10$ keV after 2 h of irradiation; thus, higher power densities deposited onto the samples. In section 4, the REBCO exhibited no discernible effects; in section 5, any degradation effects were reversible.

Rather than permanent damage to the REBCO-CC, the superconducting state could be suppressed during irradiation by Cooper pair breaking. The temporal structure of the SR mimics that of the particle beam. Consequently, the SR consists of a series of short flashes at integer multiples of the RF period [18]. The bunch spacing at the ALBA Synchrotron is 2 ns, meaning that photons with energies ranging from 10 keV to 300 keV impinge on the REBCO-CC layer every two nanoseconds. Photons with sufficient energy might break apart one or more CP which will subsequently recombine again on a time scale of $\tau_{\text{CP}} \approx 10^{-3}$–$10^{-6}$ s [35]. Assuming that all photons arriving at the sample would break a CP, since the photons arrive at the sample at a faster rate than the recombination time of CP, the statistical Cooper pairing mechanisms would be suppressed during irradiation, and the superconducting properties altered in the irradiation area. Nevertheless, the direct current transport characterisation of the critical temperature and its transition width did not indicate any change in the superconducting properties during the photon irradiation, although in the RF SR surface impedance measurements, the REBCO-CC was certainly affected. Accordingly, besides the timing structure, which is the same for both experiments, the data suggest that the SR flux intensity also plays a role. Experimentally it was determined that while there is no change in the transition temperature when using a beam current up to $I_{\text{beam}} = 200$ mA, the surface impedance of the REBCO-CC was strongly reduced above a particular threshold, which depending on the provider is around $I_{\text{beam}} =$ 120–150 mA. Comparing the photon fluxes from tables 4 and 5, which impinge on the REBCO-CC samples in different experiments as a function of varying beam currents, it can be observed that there is a visible impact in only one experiment.

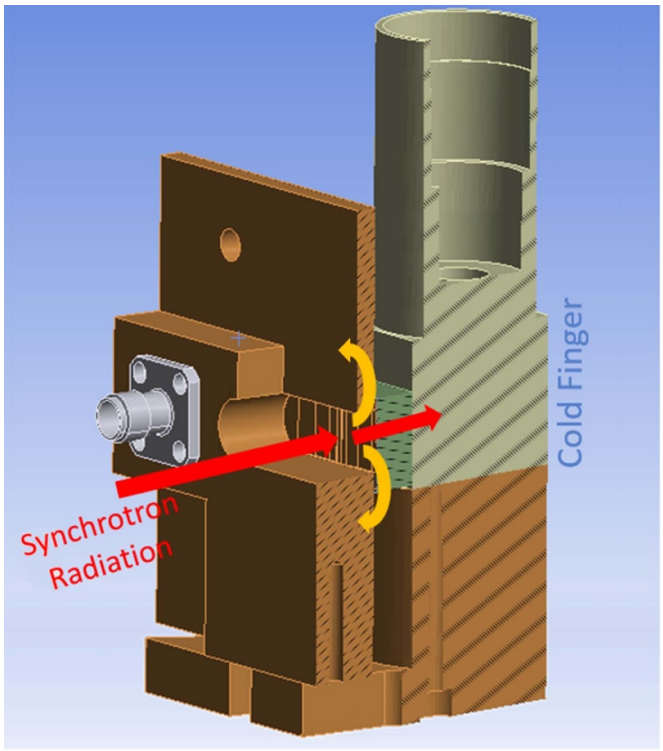

Figure 15. ANSYS simulation model of the PPR for SR power deposition.

This could potentially be attributed to the significant difference in absorbed photons between the two experiments. Thus, as it is well known that the absorption of SR leads to heat deposited on the samples and, consequently, to a temperature increase, we explored the possibility that the effects seen on the surface impedance are of thermal origin.

A steady-state thermal analysis of the PPR under photon irradiation was performed using ANSYS [37]. The numerical model is shown in the cross-sectional view in figure 15. The boundary condition for the simulation is set as follows. The cold finger is kept at a constant temperature of $T = 50\,\mathrm{K}$. On the other side of the PPR, a constant heat flux is given by an imported power map equivalent to the SR power generated by a beam current of $I_{\mathrm{beam}} = 250\,\mathrm{mA}$. The absorption of the different layers was estimated using XOP [38], and the power density distribution at each layer was determined via SYNRAD+ for SuperPower. The heat flow due to the SR is dissipated through the several layers of the PPR (delaminated REBCO-CC, dielectric and REBCO-CC) normal to the PPR (red arrows) as well as through the fixture base, i.e. parallel to the PPR (yellow arrows), as indicated in figure 15.

As the PPR is under vacuum ($\approx 10^{-5}$ mbar), the heat flow is considered purely conductive in the simulation. The heat conduction Q_{cond} can be generally expressed as [39]:

$$Q_{\mathrm{cond}} = \frac{\Delta T}{R^{\mathrm{th}}}, \tag{3}$$

where ΔT is the temperature difference, R^{th} is the heat resistance of different media through which the heat conducts. As a medium, we consider both the different materials and thermal contacts between materials. Besides, the heat flow through the PPR deals with a complex multilayered structure of nano- to micrometre thicknesses while having a millimetre scale in the other directions, which is difficult to address numerically. Therefore, the challenge of accurately meshing such thin layers has been overcome by merging layers of which we can assume perfect thermal contact properties and estimate their equivalent thermal conductivity. For example, the delaminated REBCO-CC architecture with Hastelloy, four to six buffer layers and the REBCO layer can be considered having perfect thermal contact, with an equivalent thickness of 51.8 μm (1.6+0.2+50 : REBCO+Buffer+Hastelloy) and equivalent thermal conductivity $R^{\mathrm{th}}_{\mathrm{CC},\parallel} = 6.8\,\mathrm{W\,Km^{-1}}$ parallel to the layer and $R^{\mathrm{th}}_{\mathrm{CC},\perp} = 6.9\,\mathrm{W\,Km^{-1}}$ normal to the layer. Figure 16 displays the layers that have been merged for the numerical analysis, the values of the thermal contacts used in the simulation, and the power absorbed per merged layer. Sapphire with a thickness of 250 μm is considered isotropic $R^{\mathrm{th}}_{\mathrm{sapph}} = 5000\,\mathrm{W\,Km^{-1}}$. The delaminated REBCO-CC is considered with an equivalent thickness of 23.6 μm (20+2+1.6 : Cu+Ag+REBCO) and equivalent thermal conductivity $R^{\mathrm{th}}_{\mathrm{delam},\parallel} = 663\,\mathrm{W\,Km^{-1}}$ parallel to the layer and $R^{\mathrm{th}}_{\mathrm{delam},\perp} = 48\,\mathrm{W\,Km^{-1}}$ normal to the layer. The pure copper onto which the REBCO-CCs are adhered has a uniform thickness of 5 mm, and an isotropic thermal resistance of $R^{\mathrm{th}}_{\mathrm{Cu}} = 720\,\mathrm{W\,Km^{-1}}$.

In the PPR, in order to ensure good thermal contact among the individual components, the structure was pressed together and held into place via springs. However, the thermal contact conductance C^{th} depends not only on the materials that form the contact but also on the type of contact. In this numerical study, the value of thermal contact conductance between components with $C^{\mathrm{th}}_{\mathrm{thp}}$ and without C^{th}_{p} thermal paste are considered as an input parameter in ANSYS. The software includes a panel for surface-to-surface thermal contact conductance, where values need to be specified for each layer. In each simulation we assumed that the contacts with thermal paste are equal $C^{\mathrm{th}}_{\mathrm{thp1}} = C^{\mathrm{th}}_{\mathrm{thp2}} = C^{\mathrm{th}}_{\mathrm{thp3}}$ and the contacts between REBCO layers and sapphire are equal $C^{\mathrm{th}}_{1} = C^{\mathrm{th}}_{2}$.

Figure 17 provides the numerical results obtained from the analysis of heat load deposited layer by layer. The figure shows the maximum temperature reached by each CC as a function of $C^{\mathrm{th}}_{\mathrm{thp}}$ of thermal paste and varying the contact conductance values between the REBCO layers and sapphire C^{th}. For comparison reasons, the critical temperature line is added to the graph. The findings suggest that by varying the thermal contact conductance within a range of empirically determined values for moderate pressure among ceramics, as documented in the literature [39], the temperatures of both REBCO-CCs increase. Furthermore, the findings demonstrate that the REBCO-CC behind the sapphire is more affected than the delaminated REBCO-CC due to Hastelloy's significantly lower thermal conductivity and larger thickness compared to copper, i.e. stronger power absorption. The temperature of the REBCO-CC reaches almost T_C, even in this highly simplified numerical approach. Accordingly, exchanging Hastelloy

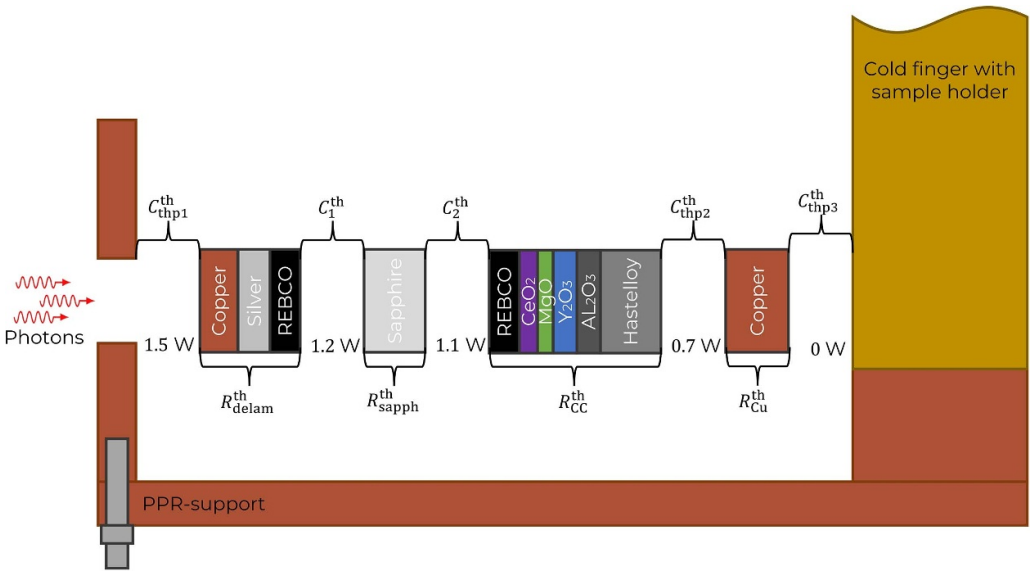

Figure 16. Sketch of the equivalent numerical PPR indicating which layers are virtually merged and added. Additionally, the SR power deposition per merged layer is given.

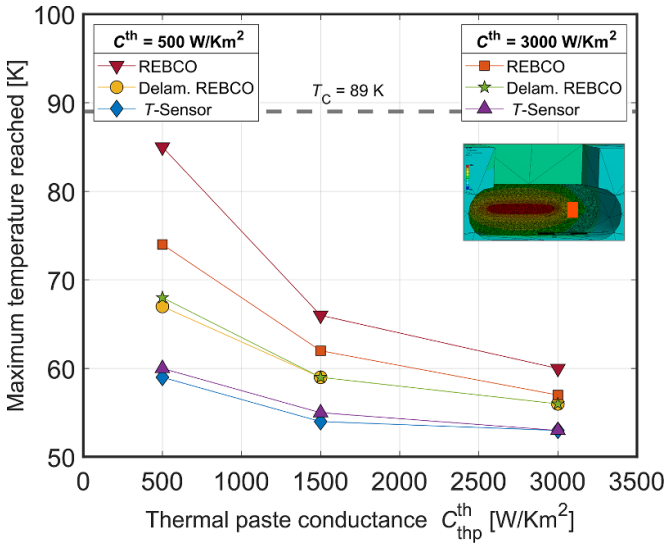

Figure 17. Synchrotron radiation power deposition results obtained via ANSYS steady-state thermal solver. The results for two thermal contact conductances are given. In addition, the critical temperature is shown (dashed line). The inset shows the temperature map at the oval cut-out of the PPR and the position of the temperature sensor (orange square).

for any better thermal conducting material will improve the temperature distribution and, thus, reduce the effect of heating. The reduced thermal conductivity of the underlying layers beneath the REBCO can also provide an explanation for the observed results in the Fujikura samples when compared to those of SuperPower's.

The inset of figure 17 presents a heat map of temperature change calculated at the delaminated sample's centre. The results show that the temperature change follows the oval cut-out profile and that the temperature increase is lower at the position of the additional temperature sensor. During the surface impedance measurements, a temperature increase between 7–10 K at the indicated position of the temperature sensor attached to the delaminated samples was measured, which is consistent with the results determined over the numerical estimations for the lowest contact conductance values. According to this data, there is a strong indication that it is not unlikely that at least one REBCO-CC or the affected area of one REBCO-CC was transitioning into the normal conducting state due to heating effects.

For the FCC-hh beam screen chamber, these results provide further support for the hypothesis that delamination of REBCO-CCs is the best approach not only to mechanically attach REBCO-CCs onto the beam screen but as well to cope with any possible heat load increase. The total power expected to be deposited on the inner beam screen is $P_{BS} = 0.6\,W$ with a maximum surface power density of $p_{BS} = 0.3\,mW\,cm^{-2}$. The maximum surface power density at the PPR is $p_{PPR} = 2.3\,W\,cm^{-2}$; thus, approximately a factor 8000 higher than in the FCC-hh. In addition, the separation between bunches at ALBA is a factor 12.5 smaller than at the FCC-hh, which means that the thermal relaxation time constants in the FCC-hh beam screen are much longer. Based on the findings, it can be reasonably assumed that the impact of SR in terms of power is not a significant concern for the hybrid FCC-hh beam screen. Consequently, it would not affect the thermal stability of a hypothetical RF-power induced thermal runaway [40].

7. Conclusion

The present study was designed to determine the effect of medium-to-high energy SR on the properties of commercially available high-temperature superconducting REBCO-CCs at cryogenic temperatures, with the main focus on the specific research work required to construct a hybrid beam screen

using REBCO-CC and Cu for the circular particle colliders of the future.

We looked into the potential long-term *ex-situ* irradiation effects caused by high-energy photons (over 80 keV) via a non-destructive technique based on a microwave resonator. REBCO-CC samples from five providers were exposed for up to 550 h, equivalent to a dose of 400 Gy. We observed that the photons did not cause damage to the REBCO layer. In addition, being exposed to air (low humidity) for four weeks does not impact the CC either. We demonstrated that the effect of irradiation on RF loss is smaller than our experimental uncertainty, and thus, we cannot detect degradation of surface resistance in irradiated samples.

We investigated *in-situ* the impact of photons with medium-to-high energy (over 10 keV) on the critical temperature and critical temperature transition width. We observed the *in-situ* SR effects on the surface impedance. First, we performed critical temperature measurements for two different REBCO-CC providers with and without SR. The resistivity measurements conducted did not indicate any changes in the critical temperature value or the width of the transition from the superconducting to the normal conducting state. In contrast, an impact of SR on the samples was detected through *in-situ* surface impedance measurements using a PPR for two providers of REBCO-CCs. The results revealed that the surface impedance increases above a certain threshold in the intensity of the SR. An average reduction of the quality factor of 40% was measured at 50 K for a deposited power density of 2.3 W cm^{-2}. This power density is almost a factor of 8000 larger than the expected power density at the FCC-hh beam screen. Reducing the SR revealed that the process is reversible. Regardless, such a change in quality factor suggests that the superconducting state is locally depressed. We have shown that the results are compatible with local heating due to SR impinging on the samples as a consequence of possible poor thermal contact. Therefore, for the FCC-hh beam screen, the system's cooling capacity must be sufficient to compensate for the heat load caused by the SR. Even though the experiments have been conducted without any magnetic field applied, the influence of the SR on the surface impedance should not change due to an applied magnetic field. Certainly, the absolute value of the surface resistance itself increases with the magnetic field strength; thus, as already mentioned, the system's cooling capacity must be sufficient to compensate for the heat load caused by the SR. Nevertheless, and within the experimental uncertainty, we cannot completely exclude that CPs are broken during irradiation, although given the involved time scales, there is strong evidence that the thermal effects mentioned are the mechanism responsible for the observed increase in surface impedance. Not only the deposited power but also the photon energy is an essential parameter for suppressing superconductivity. Thus, further studies are anticipated with lower photon energies.

In conclusion, based on the long-term exposure and the *in-situ* measurements, our findings suggest that REBCO CCs do not change their superconducting properties when exposed to the expected SR power densities of the FCC-hh. We expect that the results presented here will make it possible to improve predictions of the impact of SR on REBCO-CCs in a beam screen and stress the importance of performing detailed thermal analysis when looking into further possible applications of the REBCO-CCs in the field of future particle accelerators.

Data availability statement

All data that support the findings of this study are included within the article (and any supplementary files).

Acknowledgments

Authors acknowledge the support and samples provided by Bruker HTS GmbH, Fujikura Ltd SuNAM CO Ltd SuperOx, SuperPower Inc. and Theva Dünnschichttechnik GmbH. This work was supported by CERN under Grants FCC-GOV-CC-0072/KE3358, FCC-GOV-CC-0153/KE4106 and FCC-GOV-CC-0208/KE4947/ATS. N Tagdulang acknowledges MSCA-COFUND-2016-754397 for the PhD grant. Authors want to acknowledge Dr T Puig and Dr J Gutierrez for the fruitful discussion on photon quasiparticle interactions. We also want to thank Dr A Romanov for providing the photolitography of the samples and G Telles and Dr X Granados for providing the delamination of the samples.

ORCID iDs

Patrick Krkotić https://orcid.org/0000-0003-1892-0350
Nikki Tagdulang https://orcid.org/0000-0002-6248-0906
Sergio Calatroni https://orcid.org/0000-0002-2769-8029
Juan Manuel O'Callaghan https://orcid.org/0000-0002-2740-0202
Montse Pont https://orcid.org/0000-0003-4830-2692

References

[1] Benedikt M *et al* 2019 *Eur. Phys. J. Spec. Top.* **228** 755–1107
[2] Brüning O *et al* 2004 *LHC Design Report* (CERN)
[3] Tang J 2022 *Front. Phys.* **10** 828878
[4] Aberle O *et al* 2020 High-luminosity large hadron collider (HL-LHC) *Technical Design Report* (CERN)
[5] Zimmermann F *et al* 2019 *Eur. Phys. J. Spec. Top.* **228** 1109–382
[6] Bellafont I, Mether L, Kersevan R, Malyshev O B, Baglin V, Chiggiato P and Pérez F 2020 *Phys. Rev. Accel. Beams* **23** 043201
[7] Gan P, Zhu K, Fu Q, Li H, Lu Y, Easton M, Liu Y, Tang J and Xu Q 2018 *Rev. Sci. Instrum.* **89** 045114
[8] Krkotić P, Niedermayer U and Boine-Frankenheim O 2018 *Nucl. Instrum. Methods Phys. Res.* A **895** 56–61
[9] Puig T *et al* 2019 *Supercond. Sci. Technol.* **32** 094006
[10] Romanov A, Krkotić P, Telles G, O'Callaghan J, Pont M, Perez F, Granados X, Calatroni S, Puig T and Gutierrez J 2020 *Sci. Rep.* **10** 12325
[11] Krkotić P *et al* 2022 *Supercond. Sci. Technol.* **35** 025015
[12] Telles G T, Romanov A, Calatroni S, Granados X, Puig T and Gutierrez J 2023 *Supercond. Sci. Technol.* **36** 045001
[13] Krkotić P, Tagdulang N D, Calatroni S, O'Callaghan J M and Pont M 2022 *Europhys. Lett.* **140** 64001
[14] Xi X, Martin C, Hwang J, Lobo R S P M, Tashiro H, Zhang H, Reitze D H, Stanton C J, Tanner D B and Carr G L 2012 *J. Phys.: Conf. Ser.* **359** 012010

[15] Takahashi T 1991 *Nucl. Instrum. Methods Phys. Res.* A **303** 515–22
[16] Testardi L R 1971 *Phys. Rev.* B **4** 2189–96
[17] Romanov A 2022 Superconducting coated conductors for proton beam screens in high-energy particle accelerators *PhD Thesis* Universitat Autonoma de Barcelona
[18] Wiedemann H 2007 *Particle Accelerator Physics* 3rd edn (Springer)
[19] Walker R 1994 *Synchrotron Radiation* (CERN)
[20] Bellafont I 2020 Study of the beam induced vacuum effects in the cryogenic beam vacuum chamber of the future circular hadron collider *PhD Thesis* Universitat Politecnica de Catalunya
[21] Kersevan R and Ady M 2019 *IPAC 2019* pp 1327–30
[22] Plakida N 2010 *High-Temperature Cuprate Superconductors* (Springer)
[23] Hakki B and Coleman P 1960 *IEEE Trans. Microw. Theory Tech.* **8** 402–10
[24] Klein N, Zuccaro C, Dähne U, Schulz H, Tellmann N, Kutzner R, Zaitsev A G and Wördenweber R 1995 *J. Appl. Phys.* **78** 6683–6
[25] Krkotic P 2022 Evaluation of the surface impedance of ReBCO coated conductors and requirements for their use as beam screen materials for the FCC-hh *PhD Thesis* Universitat Politechnica de Catalunya
[26] Krkotić P, Aguasca A and O'Callaghan J 2018 *48th European Microwave Conf.* pp 882–5
[27] Arcos D, Krkotić P, O'Callaghan J M, Pont M, Ametller L and Ferrer-Anglada N 2019 *Phys. Status Solidi* b **256** 1900428
[28] Hannah A, Krkotić P, Valizadeh R, Malyshev O, Mutch J, Whitehead D, Pont M, O'Callaghan J and Dhanak V 2021 *Vacuum* **189** 110210
[29] Buckel W and Kleiner R 2013 *Supraleitung: Grundlagen und Anwendungen* (Wiley)
[30] Gorter C and Casimir H 1934 *Physica* **1** 306–20
[31] Courts S S Lake shore cryotronics (available at: www.sciencedirect.com/science/article/pii/S0011227522001989)
[32] Taber R 1990 *Rev. Sci. Instrum.* **61** 2200–6
[33] Solovyov V and Farrell P 2016 *Supercond. Sci. Technol.* **30** 014006
[34] Telles G *PhD Dissertation* private communication
[35] Day P, LeDuc H, Mazin B, Vayonakis A and Zmuidzinas J 2003 *Nature* **425** 817–21
[36] Tedrow P M, Faraci G and Meservey R 1971 *Phys. Rev.* B **4** 74–82
[37] ANSYS 2023 (available at: www.ansys.com)
[38] Sanchez del Rio M and Dejus R J 2004 *Proc. SPIE* **5536** 171–4
[39] Lienhard J 2019 *A Heat Transfer Textbook* (Dover Publications)
[40] Vaglio R and Calatroni S 2019 *Eur. Phys. J. Spec. Top.* **228** 749–54